Journal of
Materials Chemistry A

SUPPLEMENTARY INFORMATION

Magnesium Phosphate-based Thermoelectric Materials as an Efficient, Stable and Scalable Bulk Power Supply Solution

Yangzezhi Zheng,‡[a] Yulin Wang,‡[b] Yang Zhou, *[b] Weihuan Li,[b] Siyu Chen,[a] Shengjun Chen,[b] Chenchen Xiong,[b] Jiarui Xing,[b] Tao Ma,[a], and Xiaoming Huang *[a]

List of Figures

List of Tables

---

* *corresponding authors.*

[a] *School of Transportation, Southeast University, Nanjing, China.*

[b] *School of Materials Science and Engineering, Southeast University, Nanjing, China.*

‡ These two authors contributed equally to this work.

Methods

0.1 Preparation of METEMs

The reaction of MPMs[1] is based on the following chemical reaction equation:

$$MgO + KH_2PO_4 + 5H_2O = MgKPO_4 \cdot 6H_2O \tag{1}$$

Generately, MgO should be excessive to ensure optional mechanical characteristics. Hence, a mass ratio of MgO:KDP of 3.5:1 was used[2]. Firstly, all the powdered ingredients were stirred for 5 minutes, then slowly pour in the determined proportion of water for about 20-30s. After adding the water, continue stirring for 2 minutes, and then put the slurry into the designated size moulds. Finally, the specimens were demoulded after 40 minutes, and all MPTEMs were kept at 20-25 $^{\circ}C$ with 65% humidity until the required curing time.

0.2 Measurement of thermoelectric characteristics

Thermal conductivity and density were tested using the DRE-III, testing two $40 \times 40 \times 40 mm^3$ specimens of MPTEMs at a time, with each specimen tested in three directions seperately. The average of three measurements was taken as the final result.

The open circuit voltage and the temperature difference were measured and recorded simultaneously. K-type thermocouples were placed between the MPTEM and the top and bottom copper sheets, recorded by a TA612C thermometer. The voltage difference between the copper sheets is the open circuit voltage, recorded through AUTOLAB-M204 electrochemical workstation. A copper block of approximately $25 \times 25 \times 25 mm^3$ was used and placed on top to ensure the stability of the contact between devices and MPTEM. One end of the combined device was heated by a BYA-BY1515 heating table and the other side was passively cooled in air. The temperature difference between the two ends of the device was controlled by adjusting the heating temperature of the table. When the temperature difference stabilised at a specific value, the open circuit voltage would be recorded. The slope of the temperature difference versus open circuit voltage curve is the Seebeck coefficient of this MPTEM.

The demoulded $40 \times 40 \times 40 mm^3$ MPTEMs were placed between two copper sheets, then the Nyquist plots and Cyclic Voltammetry curves of the MPTEMs were tested using the electrochemical workstation. The (fitted) intersections of the Nyquist plot with the abscissa was considered as the resistance of the MPTEMs. The conductivity of the MPTEMs would be calculated using the following equation.

$$\sigma = 1/(R \times 40mm) \tag{2}$$

0.3 Structural characterization

The demolded 5.0% MPTEMs would be ground and passed through a 0.075mm sieve. Take 10 g of the powder and soak it in 20 g of deionized water for 120 h. After soaking, the liquid was filtered using a 0.22 μm filter membrane until no visible particles were present, and the filtered liquid was used for ion chromatography analysis using a Thermo Fisher Scientific ICS-5000+. After the powder and water are stirred to form a slurry, it would be immediately placed into the TAM-air to test the reactive exothermic behavior of the MPTEMs, with a 24-hour test period for each specimen.

In addition to the test methods described above, the ZEISS Sigma 300 was used for SEM and SEM-mapping tests. Microtrac S3500 was used to test the specific surface area of MgO. Thermo Fisher Scientific Nicolet iS20 was used to test the functional group structure inside the MPTEMs. YXLON Y.CT PRECISION S was used to characterize the microstructure of 5.0% MPTEM specimens.

0.4 Molecular dynamics calculations

The migration process of Mg^{2+}, K^+ and PO_4^{3-} ions within K-struvite structure were simulated through molecular dynamic simulation (MD).

The establishment of the model was based on the crystal structure proposed by Graeser[3]. Firstly, the K-struvite (001) surface was cleaved from the supercell, and a thick vacuum layer (50 Å) was put between two surface sturcutres. Subsequently, the Mg^{2+}, K^+ and PO_4^{3-} ions and water molecules were adsorbed into the pore using the Grand Canonical Monte Carlo method. The resulting model encompasses a total of 27292 atoms possessing x, y, z dimensional dimensions of approximately $55 \times 50 \times 100$ Å, and the concentration of $MgKPO_4$ solution was approximately 0.6 mol/L.

MD simulation was conducted by using LAMMPS software and the Clay Force Field (ClayFF)[4] was employed. The ClayFF was derived from the quantum mechanics and has found extensive application and validation in simulating hydrated and multicomponent mineral systems, including their interactions with aqueous solutions[5]. The force field parameters can be found in[4,6]. During the whole simulation,the temperature was set to 300K under a canonical ensemble (NVT) when the periodic boundary conditions were applied. With a timestep of 0.0005ps, the system was fistely relaxed for 100ps to reach equilibrium before another 300ps production run for statistical analysis. The mean square displacement (MSD) was calculated to characterize the thermal motion of the molecules, and the radial distribution function (RDF) was employed to characterize the interactions between K-struvite and the three ions.

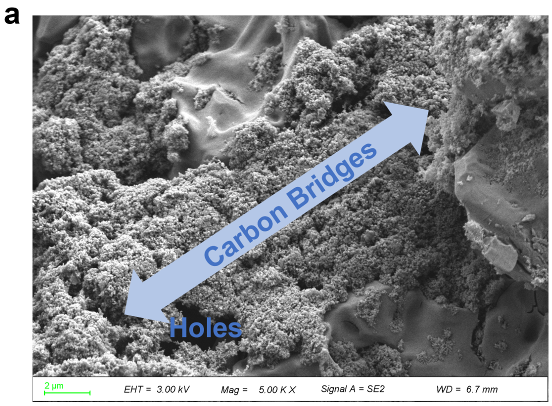

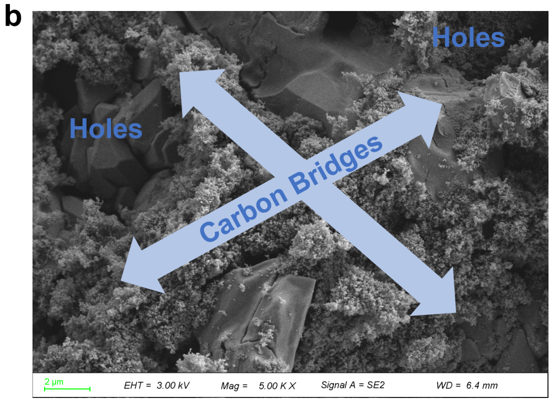

Fig. S1 Supplementary SEM image of MPTEMs.
The scale bar is 1 mm.**a** Characteristic Image 1. **b** Characteristic Image 2. The bridging effect of carbon black in MPTEMs may be unidirectional or multidirectional. This gives rise to a complex circuit structure within the MPTEMs.

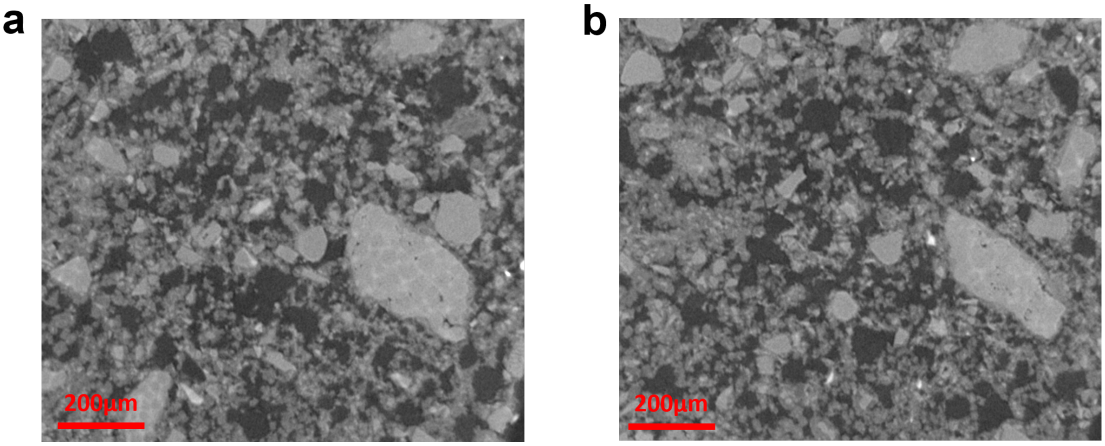

Fig. S2 Three-dimensional X-ray microscopy image of MPTEMs.
The scale bar is 200 μm. Gray scale values from lightest to darkest are: unreacted KDP, MgO, hydration products, carbon black and pores. **a**, **b** and **c** are selected from different locations of the same sample. The nano-CT is almost impossible to distinguish the pores from the carbon black, suggesting that these two are spatially distributed in the same way, and the wrapping of the i-TE units by the carbon black is quite significant. In addition, the nano-CT images revealed unhydrated KDP, but this was not found in XRD, indicating that the unhydrated KDP is extremely trace.

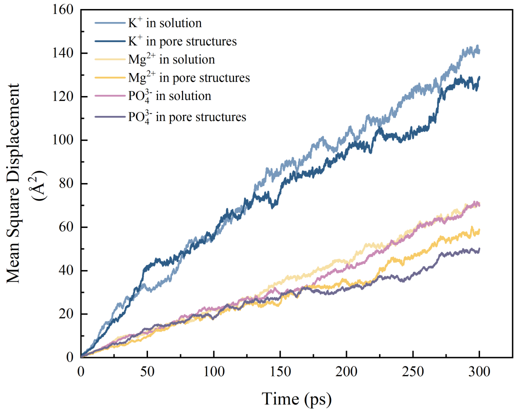

Fig. S3 The MSD of PO_4^{3-}, Mg^{2+}, and K^+ in pure solution environments and K-struvite pore solution environments with a spacing of 50 Å.

Under the influence of K-struvite crystals, the MSDs of all three ions decreased, but the rate of decrease of PO_4^{3-} was more significant, which caused a further widening of the gap between the diffusion coefficients of the three ions.

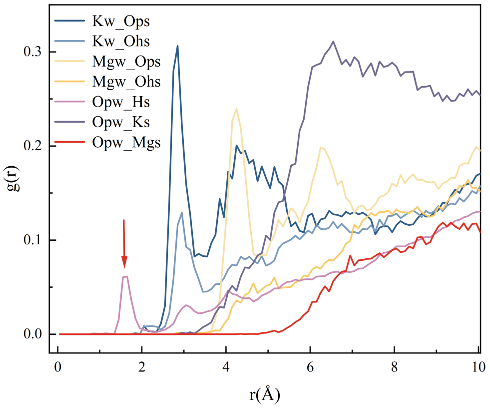

Fig. S4 Calculated RDFs between all potential bond-forming elements.

The letters preceding and following the underline represent the element in water (ion) and the element in solid (K-struvite), respectively, e.g., OpW_Hs represents the calculated RDF curve of the O in the PO_4^{3-} with the H in the K-struvite. Almost no bonding is evident for the Mg^{2+}

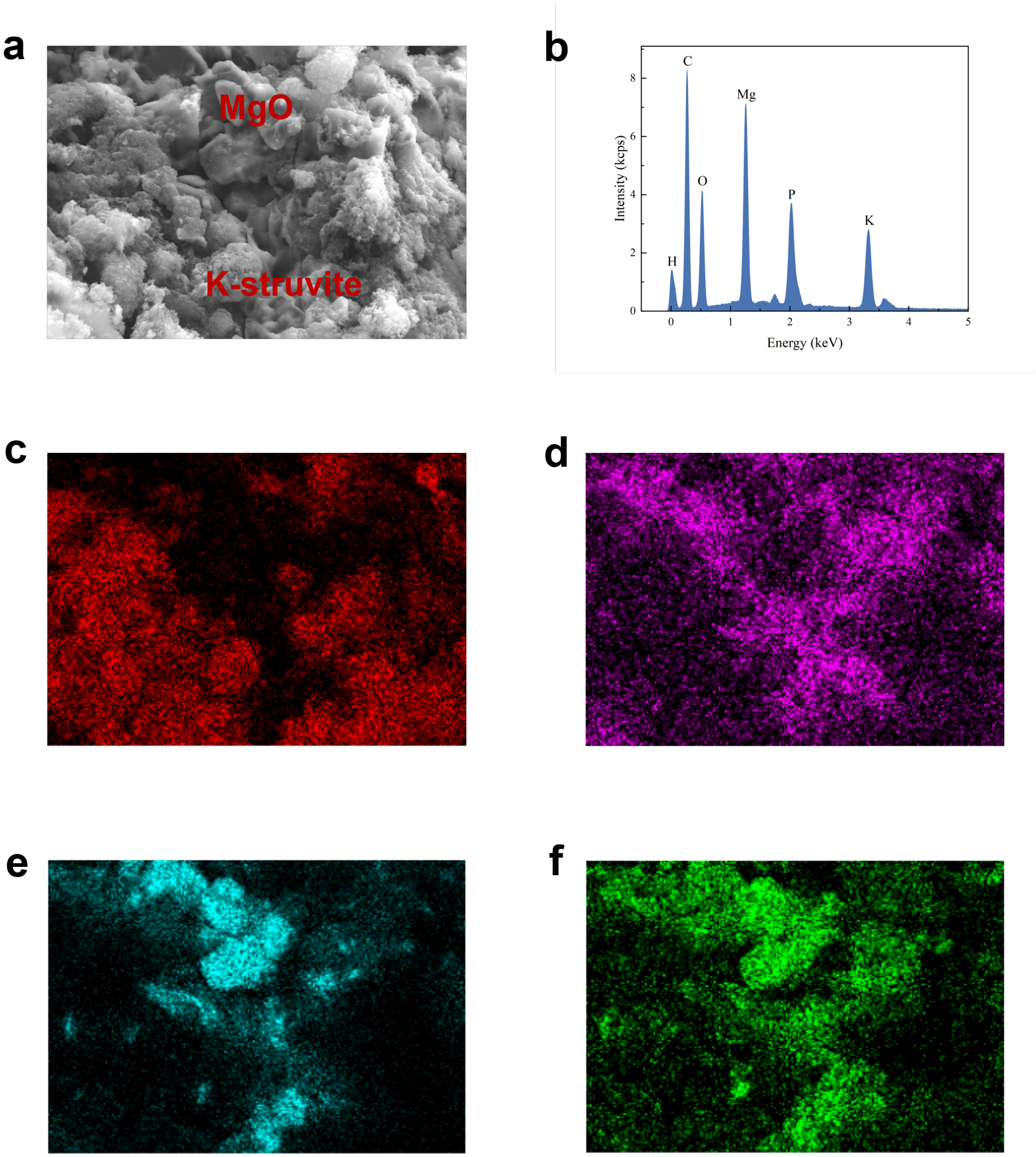

Fig. S5 SEM and EDS mapping images of MPTEMs.
Magnification 2000x. **a** SEM original image. **b** EDS spectrogram. **c** C, **d** P, **e** Mg, and **c** O elements' mappings. Carbon black is distributed on the surface of MgO and K-struvite apparently.

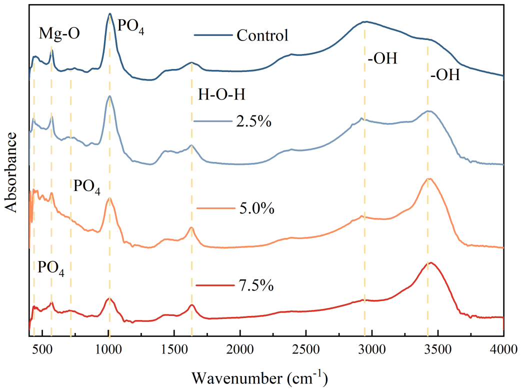

Fig. S6 FTIR curves of the MPTEMs with different carbon black dosages. The types and ratios of functional groups of MPTEMs at each doping level remained almost the same.

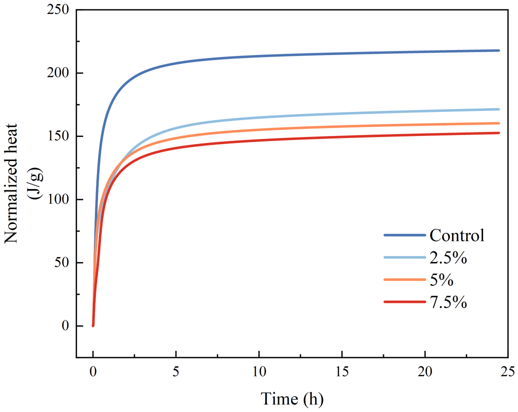

Fig. S7 Heat curves of MPTEMs under different carbon black dosages.

With the increase of carbon black content, the proportion of reactants decreases, which is more significant in the later stage of the reaction.

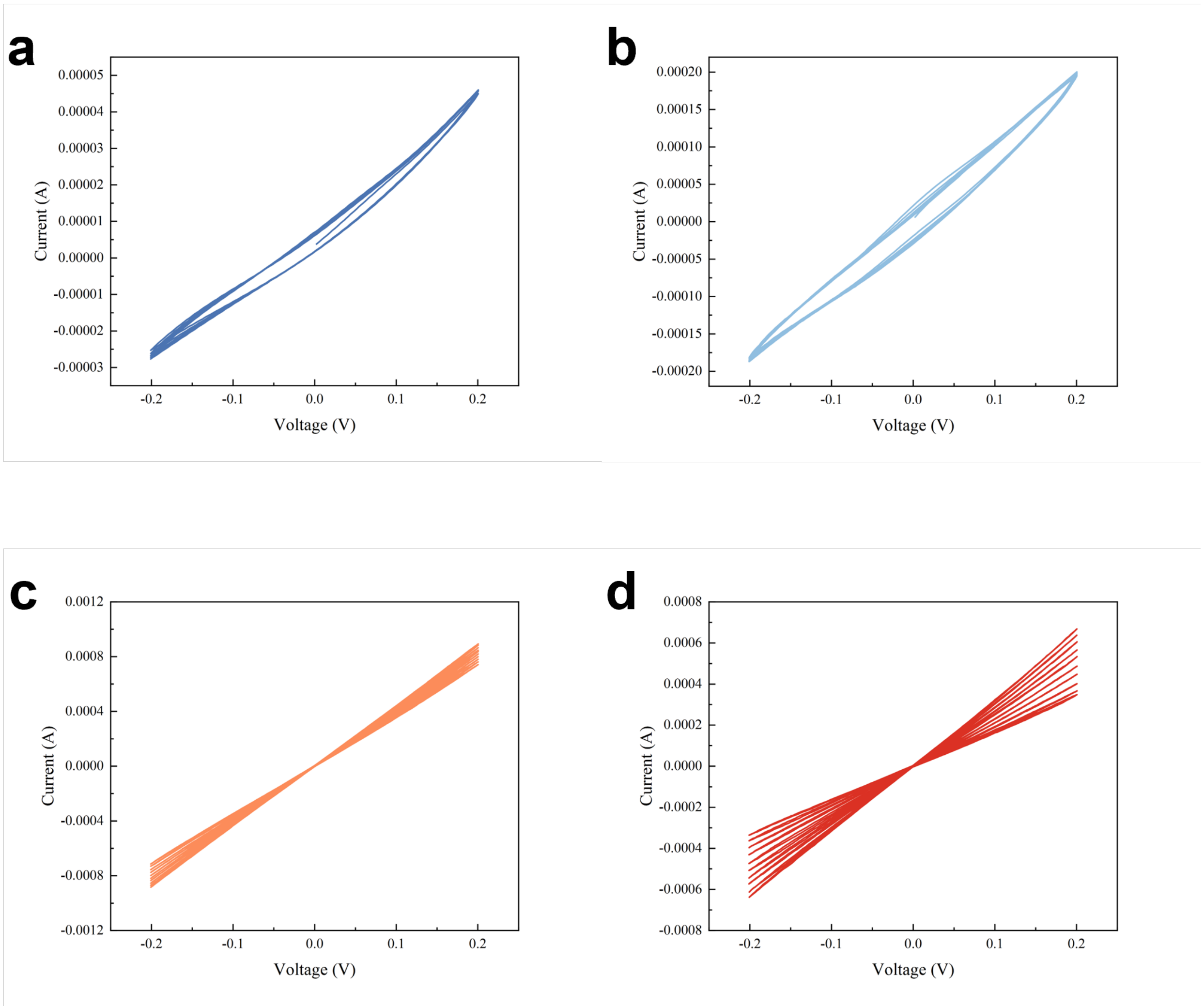

Fig. S8 Cyclic voltammograms of MPTEMs at a scan rate 10 mV/s.
a Control group. **b** 2.5%. **c** 5.0%. **d** 7.5%. No obvious redox peaks observed, suggesting that there is no redox reaction occurring within the MPTEMs.

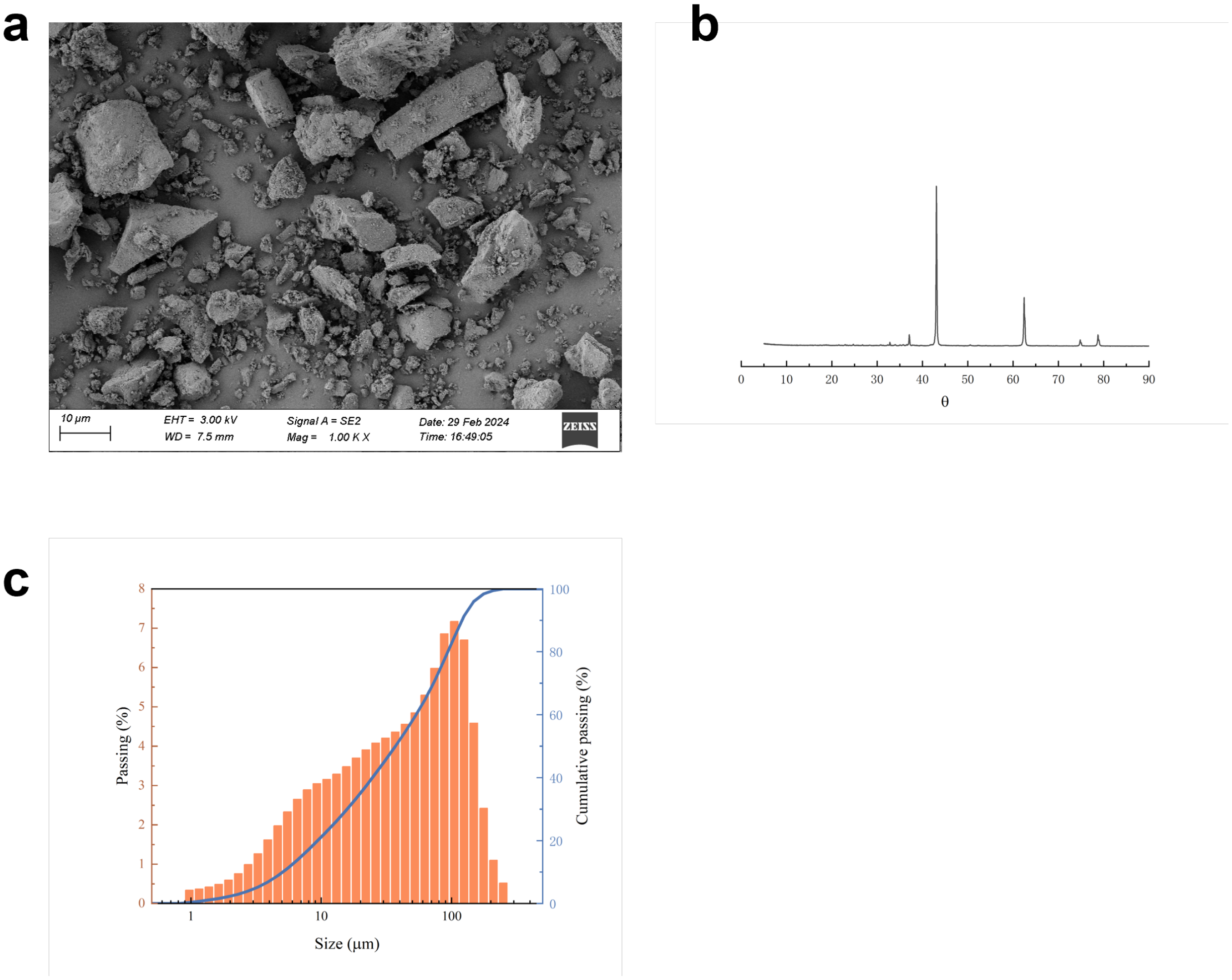

Fig. S9 Characteristics of magnesium oxide.
a SEM image.The scale bar is 10 μm. **b** XRD curve. **c** BET analysis.

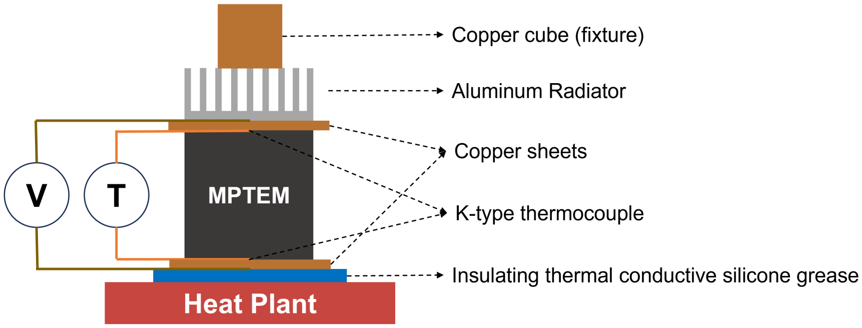

Fig. S10 Conceptual diagram of the test method for Seebeck coefficients.

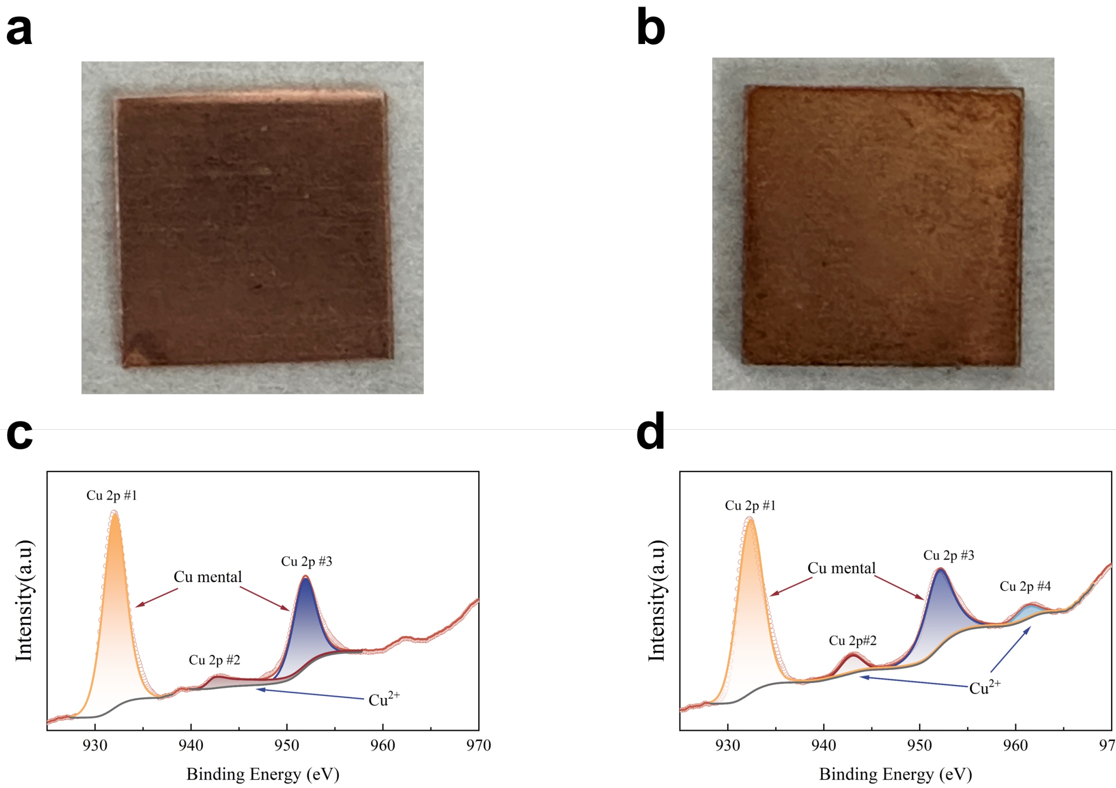

Fig. S11 Digital image of copper sheet slices ($5mm \times 5mm \times 0.05mm$) used in the experiment.

a The surface digital image of new copper sheet. **b** Heat to a temperature difference of 20 degrees between the two ends and cool naturally. Repeat this experimental step 5 times. The surface digital image of the copper sheet after cyclic testing. It can be seen that there is no obvious copper rust generated by corrosion on the surface of the copper sheet. **c** and **d** XPS test results of copper sheet surface before (**c**) and after (**c**) cycling. Trace amounts of oxides are formed when the copper sheet is heated, but the dominant surface remains the copper metals.

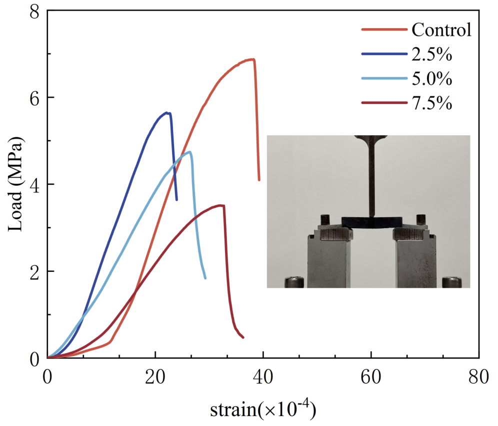

Fig. S12 Three-point bending toughness of MPTEMs.

As the MPC material itself is relatively well bonded, the MPTEMs still demonstrate a toughness superior to that of many construction materials, even with 7.5% carbon black doping.

Table S1 Raw material mixing ratios of MPTEMs.

Name	MgO	KDP	Borax	Carbon black	Water
2-6	(g)	(g)	(g)	(g)	(g)
Control	350	100	21	0	72
2.5%	350	100	21	11.25	157.5
5.0%	350	100	21	22.50	225
7.5%	350	100	21	33.75	315

Table S2 Specific surface area and density of raw materials.

Item	Specific surface area	Density
2-3	m^2/g	g/cm^3
MgO	1.2410	3.580
KDP	0.3515	2.238
Carbon Black	1297.1135	0.135

Table S3 Thermoelectric performance parameters of MPTEMs.

Dosage	Seebeck coefficient	Conductivity	Thermal conductivity	Power factor	ZT
2-6	(mVK^{-1})	Sm^{-1}	$(Wm^{-1}K^{-1})$	$(\mu Wm^{-1}K^{-2})$	
Control	3.28	0.014	1.03	0.1509	4.37×10^{-5}
2.5%	5.55	1.32	0.82	40.67	0.015
5.0%	11.16	10.42	0.74	1298	0.523
7.5%	10.72	13.16	1.23	1513	0.367

Table S4 Ingredients of magnesium oxide.

No.	Item	Results (%)
1	MgO	92.66
2	SiO_2	2.37
3	CaO	1.44
4	Fe_2O_3	1.38
5	Al_2O_3	0.79
6	Loss	1.54

References

1 S. A. Walling and J. L. Provis, *Chemical reviews*, 2016, **116**, 4170–4204.

2 M. Le Rouzic, T. Chaussadent, L. Stefan and M. Saillio, *Cement and Concrete Research*, 2017, **96**, 27–41.

3 S. Graeser, W. Postl, H.-P. Bojar, P. Berlepsch, T. Armbruster, T. Raber, K. Ettinger and F. Walter, *European Journal of Mineralogy*, 2008, **20**, 629–633.

4 R. T. Cygan, J.-J. Liang and A. G. Kalinichev, *The Journal of Physical Chemistry B*, 2004, **108**, 1255–1266.

5 Y. Li, G. Zhang, D. Hou and Z. Wang, *Construction and Building Materials*, 2021, **276**, 122213.

6 T. M. Alam, J.-J. Liang and R. T. Cygan, *Physical Chemistry Chemical Physics*, 2000, **2**, 4427–4432.